




Vacuum-Synthesized, pH-Responsive Barley-Based Microgels for Targeted Doxorubicin Delivery: Formulation and Cytotoxicity Evaluation

Anamika Ramchaik¹, Kiran Kumar^{1,*} , Sunita Ranote² , Ghanshyam S Chauhan¹ , Sandeep Chauhan^{1,*} 

¹ Department of Chemistry, Himachal Pradesh University, Summer Hill, Shimla, Himachal Pradesh, India

² Centre of Polymer and Carbon Materials, Polish Academy of Sciences, 34. M. Curie-Skłodowska St., 41-819 Zabrze, Poland

* Correspondence: drkiran@hpuniv.ac.in (K.K.); drschauhan@hpuniv.ac.in (S.C.);

Received: 7.11.2024; Accepted: 25.07.2025; Published: 9.08.2025

Abstract: An effective way to treat cancer is by designing environment-sensitive drug-loading-delivery platforms for anticancer drugs. The use of biocompatible polymer is an emerging area in this field, where the polymeric matrix is designed to deliver the selected drug to a specific targeted area. Herein, we report the *in-vacuum* synthesis of pH-responsive microgels, derived from whole-grain barley and 2-acrylamido-2-methylpropanesulfonic acid by means of free radical polymerization. The characterization of microgels was performed employing different characterization techniques, including swelling behaviour studies. The microgel showed superabsorbent behaviour with a maximum %swelling of 16,239% at 45°C and 14,449% at 37°C, within 210 min. As the swelling of the microgel was pH-responsive, it was further evaluated for controlled delivery of doxorubicin (DOX), an anticancer drug. The microgel showed appreciable loading efficiency for doxorubicin (92.23%). *In vitro*, release studies at varied pH also revealed the pH-sensitive release pattern of the microgel with a maximum release of 93.5% at pH 5.5 at 37°C. The kinetic study revealed that the DOX discharge from the microgel follows the First-order kinetic model. The cytotoxic studies on the doxorubicin-loaded microgels were performed on the lung cancer cell line (A549) using the NRU assay. The results showcase the synthesized microgel as an ideal matrix for the site-specific delivery of DOX.

Keywords: biopolymer; sustained release; nanocarrier; natural polymer.

© 2025 by the authors. This article is an open-access article distributed under the terms and conditions of the Creative Commons Attribution (CC BY) license (<https://creativecommons.org/licenses/by/4.0/>), which permits unrestricted use, distribution, and reproduction in any medium, provided the original work is properly cited. The authors retain copyright of their work, and no permission is required from the authors or the publisher to reuse or distribute this article, as long as proper attribution is given to the original source.

1. Introduction

Regardless of extensive progress in cancer treatment, it is still the second most lethal disease globally [1, 2]. According to the International Agency for Research, cancer alone led to 9.8 million deaths in 2018 [3]. Nearly 70% of all deaths due to cancer are estimated to occur in developing countries alone [4]. In India, cancer accounts for 9% of annual fatalities [5]. Cancer starts mostly with oncogenic gene mutations, which initiate the unrestrained production of cancerous cells, leading to cluster or tumour formation [6, 7]. A part of the tumour cells may split and migrate to various parts of the body via the body's lymphatic system (bloodstream) and propagate cancer [8, 9].

Presently, cancer treatment is constantly evolving with new findings and breakthroughs changing the entire course of cancer treatment. The most prevailing treatment for treating cancer is chemotherapy, involving drugs to inhibit or suppress the rapidly multiplying cancerous cells [10, 11]. It is the widely used first-line treatment for cancer. Chemotherapy not only destroys cancerous cells but also prevents their recurrence. The treatment shrinks the tumour before its removal with surgery, prevents its spreading, and makes surgery even more effective [12]. A wide range of anticancer drugs belonging to varied groups e.g., carboplatin and cisplatin drugs containing alkylating agents is employed in the treatment process [13, 14], 5-fluorouracil belonging to the antimetabolites category [15, 16] and anthracyclines e.g., doxorubicin (DOX), and daunorubicin are highly effective anti-tumour antibiotic drugs [17-19]. Doxorubicin, a significant and effective chemotherapeutic agent, is often used in treating a wide range of cancers. It works by inhibiting enzymes polymerase and topoisomerase associated with cancerous cell proliferation [20-22].

Despite being the most effective cancer treatment, chemotherapy lacks the specificity for cancerous cells, which means that it not only destroys cancerous cells but also harms healthy cells [23, 24]. The chemotherapeutic drugs are non-specific and thus a minute fraction of the administered drugs (0.1-1%) reaches the cancerous or desired site, and the rest attack the normal cells [25]. Such a low rate of drug administration necessitates administering high doses of drugs so that the therapeutic drug dose can reach the targeted site to inhibit the action of cancerous cells. But these high doses not only act on normal cells but also initiate bone marrow suppression, nephrotoxicity, neurotoxicity, cardiomyopathy, drug resistance, etc. [26, 27]. Thus, chemotherapy for cancer treatment is massively compromised by its cumulative dose-dependent side effects [28, 29]. Therefore, it is necessary to boost the delivery of the drug to affected cells to its therapeutic dosage without affecting normal cells. Designing novel drug delivery devices capable of showing the controlled release of the drug specifically at the targeted region might help the cause. In the recent years, researchers have been working to design a wide range of polysaccharide-derived carriers for site-specific delivery of anticancer drugs [30-32]. Polysaccharide-derived carriers are biodegradable, biocompatible, and non-toxic, and these properties enhance their value in the medicinal world even more. The hydrogels derived from polysaccharides are considered the most desirable carriers for targeted drug delivery due to some exceptional structural attributes such as high surface area, smart swelling properties, and negligible interfacial drag due to the reduced friction with body tissues. The pH-responsive behaviour of these hydrogels is one such important property that makes them quite suitable for the sustained delivery of drugs at the desired rate to a specific site [33-36]. The hydrogels with enhanced properties can be obtained by converting them into small-sized nanogels and microgels [37-39]. The pH sensitivity of these microgels can be exploited in anticancer therapy due to variations in the pH of the tumour in comparison to normal cells. This marks the foundation for the design of stimuli-responsive drug carriers for sustained anticancer drug release [40, 41]. Herein, we have used whole grain barley to develop such pH-responsive microgel using a free radical polymerisation reaction in vacuum. Almost 2% of the barley produced annually is used for human consumption, and the rest is used as cattle feed or wasted. Barley (*Hordeum vulgare* L.) contains mainly starch (70 %), about 15% of proteins, and a fine amount of β -glucan as its constituents [42, 43]. The presence of a high fraction of polysaccharide units, biocompatibility, and high abundance make it a good choice for functionalization and drug delivery applications.

Taking into consideration the above discussion, the current paper describes the in-vacuum synthesis of novel microgels using whole grain barley polysaccharide, AMPSA, and N, N'-methylenebisacrylamide (N, N'-MBA) via free radical polymerization. The use of 2-acrylamido-2-methylsulfonic acid (AMPSA) is preferred as it is biocompatible, and $-SO_3H$ groups in the structure can enhance the swelling properties of polymeric materials, which is quite an essential feature for drug delivery applications [44, 45]. The in-vacuum synthesis is chosen over the in-air synthesis of the hydrogel as the former can result in a higher %grafting (P_g) than the latter [46]. The synthesized microgels were characterized using Fourier transform infrared spectroscopy (FTIR), field-emission-scanning electron microscopy (FESEM), energy-dispersive X-ray spectroscopy (EDS) mapping, transmission electron microscopy (TEM), X-ray diffraction analysis (XRD), and dynamic-light scattering studies (DLS). The swelling studies were then performed at varied times and temperatures to depict the swelling capacity of the microgel. The superabsorbent microgels were further explored for site-specific and controlled delivery of an anticancer drug, doxorubicin (DOX). Various kinetic models, namely the Zero-order kinetic model, First-order kinetic model, Korsmeyer-Peppas kinetic model, and Higuchi kinetic model, were studied to establish the mechanism for delivery of doxorubicin to the targeted region. Further, the cytotoxicity of DOX-loaded microgel was investigated using a human lung carcinoma cell line (A549 cell line) and determined by NRU Assay. To the best of the authors' knowledge, no analogous work showing such a synthesis of whole grain barley-based superabsorbent microgel for controlled delivery of DOX has been reported earlier.

2. Materials and Methods

2.1. Materials.

Finely ground whole barley grain (B^{gr}) powder, AMPSA, potassium peroxodisulphate (KPS) [SISCO Research Laboratories Pvt. Ltd.], N, N'-Methylenebisacrylamide (N, N'-MBA), dimethyl sulfoxide (DMSO), hydrochloric acid (HCl), sulphuric acid (H_2SO_4), sodium hydroxide (NaOH), (S.D Fine-Chem Ltd., Mumbai, Maharashtra, India), Doxorubicin hydrochloride (DOX, Samarth Life Sciences Pvt. Ltd., Mumbai, Maharashtra, India), buffer tablets [Qualikems Fine Chem. Pvt. Ltd. Vadodra India], Dulbecco's Modified Eagle's Medium (DMEM), Neutral red uptake assay (NRU), streptomycin, penicillin and fetal bovine serum (FBS) (Hi-Media Lab. Pvt. Ltd., Mumbai, Maharashtra, India), human lung carcinoma cell line A549 (National culture for cell science, Pune, Maharashtra, India). All chemicals involved were of analytical grade. Double-distilled water was considered for the whole experiment.

2.2. Synthesis of micro-poly(Amp)-cl- B^{gr} -IV.

Whole barley grain powder (B^{gr}) was sun-dried for 12h at 40°C. Dried B^{gr} was then ground to get a fine powder. Powdered B^{gr} was soaked for 12h in double-distilled water. Afterwards, the water-soaked B^{gr} and AMPSA were taken in a ratio of 1:1 and mixed thoroughly. To initiate the reaction, N, N'-MBA (1%), and KPS (1%) were added to the above mixture. The contents of the mixture were mixed properly and kept in a vacuum oven at 75°C and 200 mmHg for 50 min. The hydrogel, poly-(Amp)-cl- B^{gr} -IV, thus formed, was washed repeatedly with ethanol and then with distilled water. The hydrogel was then equilibrated by keeping it in double-distilled water for 24 h. The equilibrated hydrogel was left to dry inside the oven kept at 40°C to get the net dry constant weight [47]. Further, a 5% solution of poly-

(Amp)-cl-B^{gr}-IV was prepared, and 100 mL of 2.5 M NaOH was added to this solution. This mixture was stirred using a magnetic stirrer (Century Electronic Stirrer CS 2006) for 5h at 40°C. This leads to partial hydrolysis of the polymer, giving shorter chains of poly-(Amp)-cl-B^{gr}-IV. The partially hydrolysed poly-(Amp)-cl-B^{gr}-IV chains obtained were precipitated out and washed thoroughly with methanol and distilled water. The dried poly-(Amp)-cl-B^{gr}-IV fragments were finally sonicated using a Cole Parmer 8890 Sonicator for 24h at 45°C. Afterwards, it was centrifuged at a speed of 15,000 rpm for 6 hours to collect the sediments of microgels. The synthesised microgels, namely micro-poly-(Amp)-cl-B^{gr}-IV, were then oven-dried at the optimum temperature.

2.3. Characterization.

The microgel, micro-poly-(Amp)-cl-B^{gr}-IV, was characterized using Fourier transform infrared spectroscopy (FTIR), Field Emission Scanning Electron Microscopy (FESEM), energy dispersive x-ray spectroscopy (EDS) mapping, high-resolution transmission electron microscopy (HRTEM), dynamic-light scattering studies (DLS), and X-ray diffraction analysis (XRD). The FTIR spectra were taken with a Perkin Elmer spectrophotometer employing KBr beads. To determine the morphological differences occurring on the surface during the reaction, FESEM and EDS studies were performed employing a HITACHI SEM 8010. High-resolution TEM images were taken on a Jeol 2100. The particle size of the microgel has been analyzed using dynamic light scattering studies using the Litesizer 500 (BM10) instrument. Transition in amorphous and crystalline phases on the surface of the backbone during polymerization was scanned using a Phillips PAN Analytical XPERT-PRO X-ray diffractometer.

2.4. Swelling studies of micro-poly-(Amp)-cl-B^{gr}-IV.

Investigation of the swelling behavior of the synthesized microgel was performed using the gravimetric method. In this method, 0.01g of the sample was taken, immersed in 50 mL of distilled water, and weighed after specific intervals, till persistent weight was reached. The weight was measured on an electronic Ohaus weighing balance. The response of the sample against different temperatures (20°C- 55°C) and different pHs (2.2, 5.5, 6.8, 7.4, 9.2, and 10.0) was also investigated. The %swelling (Ps) was calculated using a well-reported expression [48].

2.5. Loading of doxorubicin onto micro-poly-(Amp)-cl-B^{gr}-IV.

The standard solution of 300 mg/L doxorubicin (DOX) was prepared at pH 7.4 (maintained using phosphate buffer saline (PBS) and distilled water). A microgel (100mg) was submerged in 100 mL of the drug solution, and the drug engulfed by it was determined by recording the absorbance of the drug solution for measuring the remaining drug after regular intervals using a UV-visible spectrophotometer at λ_{max} – 495 nm. After the optimal drug loading, the drug-loaded sample was filtered and washed using distilled water and dried at 35°C. The drug loading efficiency was measured in terms of %uptake (%U) and was calculated as: [49]

$$\%U = C_o - C_t / C_o \times 100 \quad (1)$$

Where C_o is the concentration of total drug uptake that took place in optimum time, C_t is the drug left in solution (mg/L) at time 't'.

2.6. In vitro drug release studies.

The release of DOX from the microgel was investigated at different pH levels (7.4, 6.8, and 5.5) at 37°C to mimic the physiological pH of the intracellular compartment of lysosomes and endosomes of tumour cells (pH-5.5), extracellular pH in tumour tissues (pH-6.8), and the physiological pH of normal tissue (pH-7.4). The drug-loaded sample (100mg) was kept in a 100 mL solution of specific pH, and the drug released was measured at regular time intervals with a UV-spectrophotometer at 495 nm wavelength. The fraction of drug released was calculated as %drug release (P_r) by applying the following equation: [50, 51]

$$P_r = C_e/C_o \times 100 \quad (2)$$

Here, C_e indicates [DOX] liberated in time t , whereas C_o is the total [DOX] engulfed by micro-poly-(Amp)-cl-B^{gr}-IV.

2.6.1. Kinetics of DOX release.

Zero order kinetic model, first order kinetic model, Korsmeyer–Peppas and Higuchi kinetic model, were computed to investigate the drug release behaviour of DOX-loaded micro-poly-(Amp)-cl-B^{gr}-IV [52]. The particulars of these models are shown in Table 1.

Table 1. Kinetic models for defining the release behaviour.

Release models	Equation	Parameters
Zero-order	$Q_t = Q_0 + k_0 t$	Q_t = drug amount released in time “ t ” Q_0 = Total drug loaded onto the sample K_0 = Rate constant calculated for zero-order.
First-order	$\log Q = \log - Q_0 - \frac{k_1}{2.303}$	Q = drug amount left at time “ t ” K_1 = Rate constant calculated for first-order.
Higuchi	$Q_t = k_H t^{1/2}$	k_H = Rate constant calculated for the Higuchi kinetic model
Korsmeyer-Peppas	$Q_t = k_{kp} t^n$	Q_t = drug amount released in time “ t ” K_{kp} = Korsmeyer-Peppas constant. n = drug release exponent

2.7. Anti-tumour activity studies.

Anti-tumour activity of micro-poly-(Amp)-cl-B^{gr}-IV was determined employing a Neutral red dye assay for the A549 lung carcinoma cell line.

2.7.1. Anti-tumour activity assay.

The cytotoxicity of the micro-poly-(Amp)-cl-B^{gr}-IV on A549 cells was determined by Neutral Red Dye Uptake (NRU) Assay. The 96-well plates were employed in culturing of cells (5000-8000 cells/well) in DMEM medium (AT149-1L) supplemented with 1% antibiotic solution and 10% FBS (HIMEDIA-RM 10432) at 37°C in the presence of CO₂ (5%). This medium was replaced after 24 h with a new culture medium added to each well of the plate. This step was followed by the addition of 5 µL of treatment dilutions (of different concentrations) to well-defined wells and incubated for 24 h. 100 µL of NR (neutral red) dye (40 µg/mL in PBS) was added to the defined wells and incubated (Heal Force-Smartcell CO₂ Incubator-Hf-90) for 1 h. The medium was removed, and NRU was mixed with 100 µL of NRU Destain solution. Finally, the plates were read at 550/660 nm using an ELISA Plate Reader (iMark BioRad-USA). IC₅₀ was calculated by using GraphPad Prism-6 software. The

cell viability (%), i.e., growth inhibitory ratio, was calculated using the following equation: [53]

$$\text{Cell viability (\%)} = \frac{A(\text{Sample})}{A(\text{Control})} \times 100 \quad (3)$$

Where A (Sample) and A(Control) represent absorbance by untreated and treated cells, respectively. The A549 cells treated with micro-poly-(Amp)-cl-B^{gr}-IV were inspected using the inverted microscope (Inverted Microscope, Hund Wilovert S, Wetzlar, Germany). Studies of assay experiments were done in triplicate.

3. Results and Discussions

3.1. Synthesis of micro-poly-(Amp)-cl-B^{gr}-IV.

B^{gr} and AMPSA-derived hydrogel experienced large variations in the value of % swelling and % grafting under different reaction conditions. The optimization of different reaction parameters, viz., time (min), vacuum (mmHg), concentration of monomer AMPSA (mol/L), and crosslinker N, N'-MBA (mol/L), was done. The different optimized parameters for the synthesis of micro-poly-(Amp)-cl-B^{gr}-IV are presented in Table 2. The optimized reaction conditions were 70 min, 200 mmHg, and 75°C. A plausible mechanism of micro-poly-(Amp)-cl-B^{gr}-IV synthesis is shown in Scheme 1.

Table 2. Optimization of reaction parameters for the synthesis of micro-poly-(Amp)-cl-B^{gr}-IV.

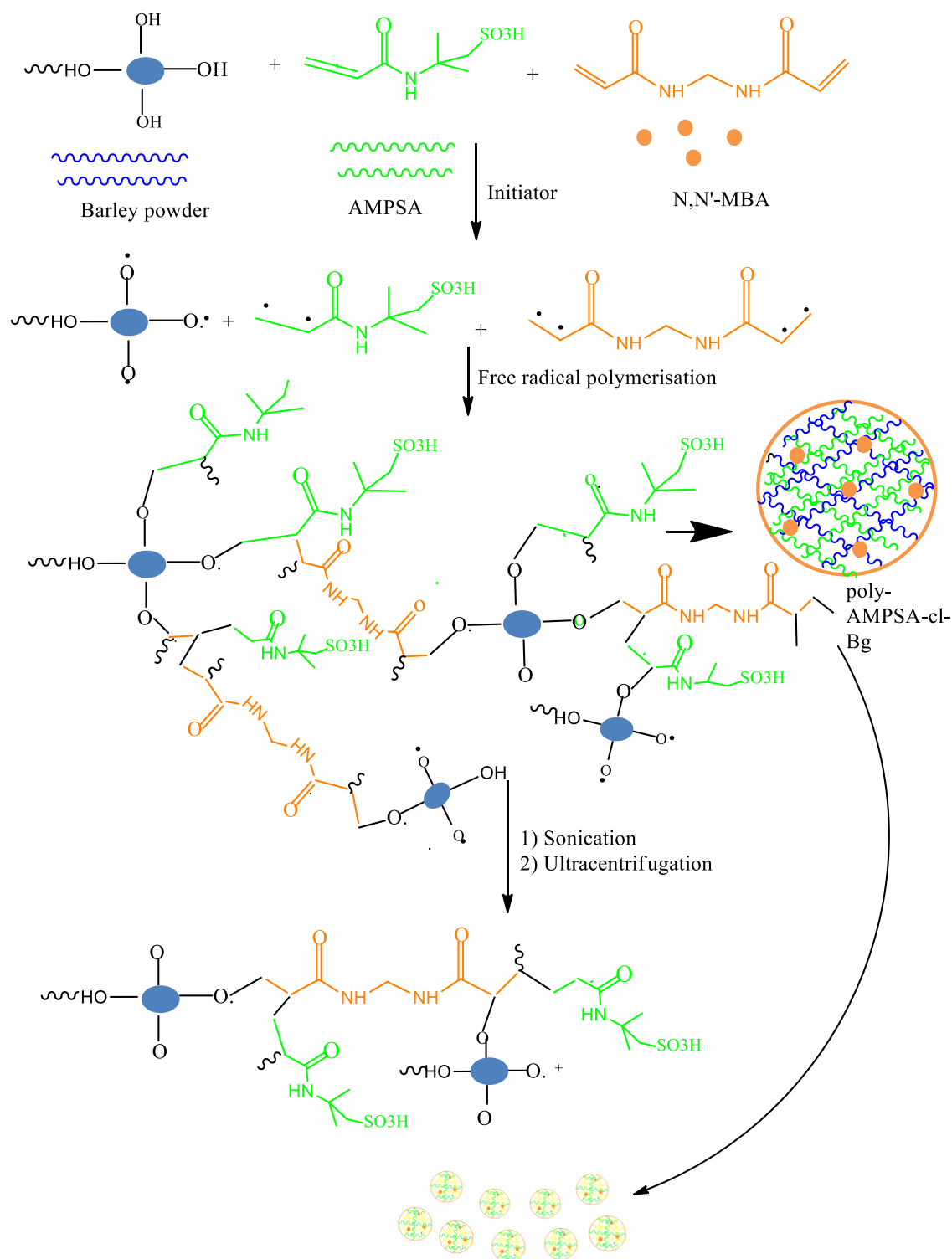
S.No.	Reaction time (min)	Reaction temp. (°C)	Vacuum (mmHg)	Monomer conc. (mol/L)	Crosslinker conc. (mol/L)	%Graftin g (P _g)	%Swelling (P _s)
1	40	70	100	4×10^{-3}	6×10^{-2}	70	-
2	40	75	100	4×10^{-3}	6×10^{-2}	82	-
3	40	80	100	4×10^{-3}	6×10^{-2}	73	-
4	40	75	200	4×10^{-3}	6×10^{-2}	89	-
5	40	75	300	4×10^{-3}	6×10^{-2}	79	-
6	50	75	200	4×10^{-3}	6×10^{-2}	93	8686
7	60	75	200	4×10^{-3}	6×10^{-2}	83	-
8	50	75	200	2×10^{-2}	6×10^{-2}	0	-
9	50	75	200	9×10^{-2}	6×10^{-2}	48	-
10	50	75	200	4×10^{-3}	3×10^{-2}	-	3400
11	50	75	200	4×10^{-3}	7×10^{-2}	-	3786

no. of replications=03; weight of B^{gr} = 1.00 g.

3.2. Characterization studies.

3.2.1. FTIR analysis.

B^{gr}, micro-poly-(Amp)-cl-B^{gr}-IV, and DOX-loaded-micro-poly-(Amp)-cl-B^{gr}-IV were characterized using FTIR, and their FTIR spectra were compared (Figure 1). B^{gr} spectrum showed a broad band between 3500– 3200 cm⁻¹ corresponding to free –OH and –NH groups [54]. The peak equivalent to 2925 cm⁻¹ in the spectrum of B^{gr} is due to -CH stretching vibration [55]. The area in the spectrum between 1200 cm⁻¹ and 1100 cm⁻¹ corresponds to hemicellulose and cellulose, respectively [56]. The 1154 cm⁻¹ peak in the spectra is attributed to asymmetric stretching of the C-O-C linkages of the β glycosidic ring [57]. The bands corresponding to 1620 and 1640 cm⁻¹ can be due to the protein substitutes in B^{gr} [58].



Scheme 1. A plausible mechanism of micro-poly-(Amp)-cl-B^{gr}-IV synthesis.

The spectrum recorded for micro-poly-(Amp)-cl-B^{gr}-IV showed peaks at 1112 cm⁻¹ and 1036 cm⁻¹, specifically that reflects the presence of S=O bonds [59, 60]. The peak at 1112 cm⁻¹ reflects the stretching vibration of the S=O bond, whereas the 1036 cm⁻¹ peak denotes the asymmetric stretching vibration of the S=O bond. These peaks signify the appreciable merging of AMPSA into B^{gr}. The reduced intensity of some peaks in the spectra of DOX-loaded micro-poly-(Amp)-cl-B^{gr}-IV was observed. The decrease in band intensity of 1112 cm⁻¹ and 1036 cm⁻¹ bands also supports considerable loading of DOX on the sample. Thus, FTIR spectra collected for micro-poly-(Amp)-cl-B^{gr}-IV and DOX-loaded micro poly-(Amp)-cl-B^{gr}-IV prove appreciable loading of DOX by the microgel [61].

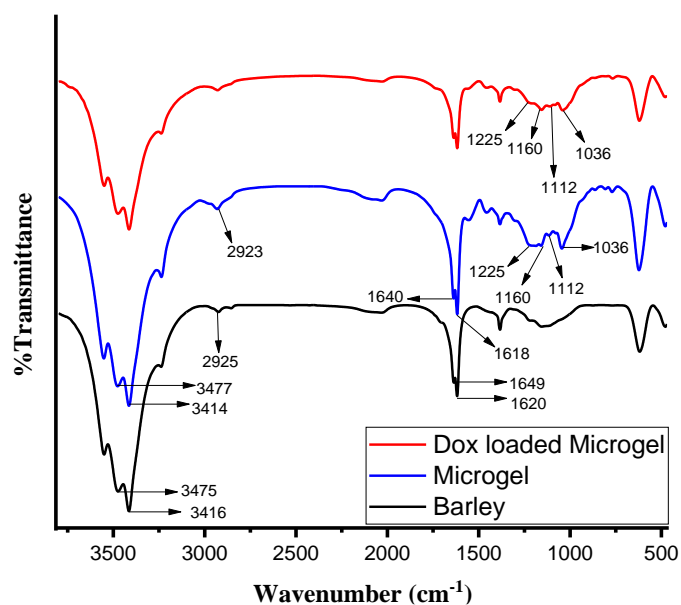
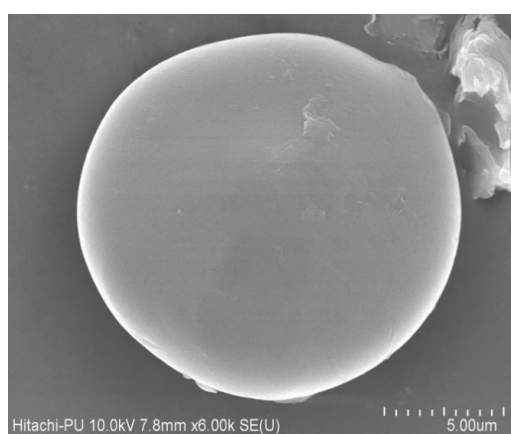


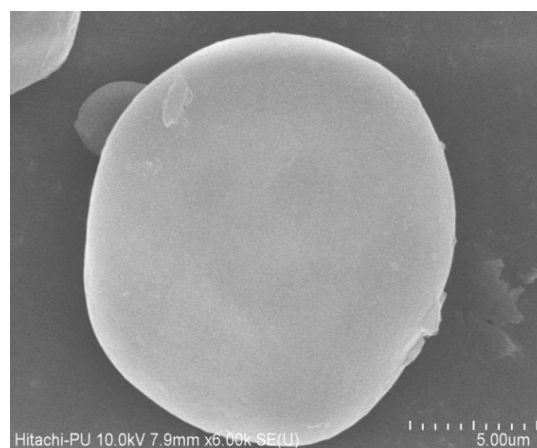
Figure 1. FTIR spectrum of B^{gr}, micro-poly-(Amp)-cl-B^{gr}-IV, and DOX-loaded micro-poly-(Amp)-cl-B^{gr}-IV.

3.2.2. FESEM-EDS studies.

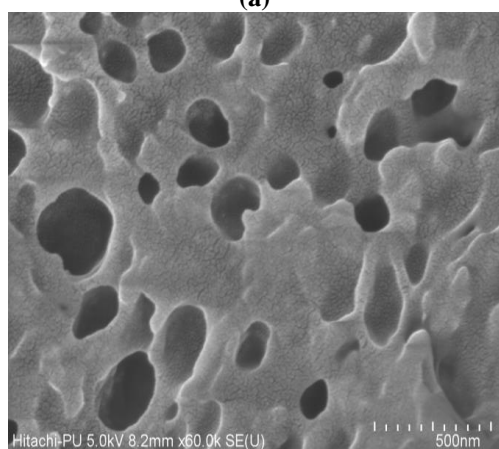
FESEM studies revealed the surface morphology of B^{gr}, micro-poly-(Amp)-cl-B^{gr}-IV, and DOX-loaded-micro-poly-(Amp)-cl-B^{gr}-IV.



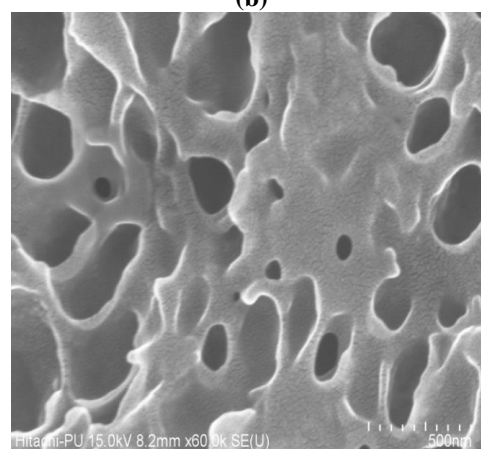
(a)



(b)



(c)



(d)

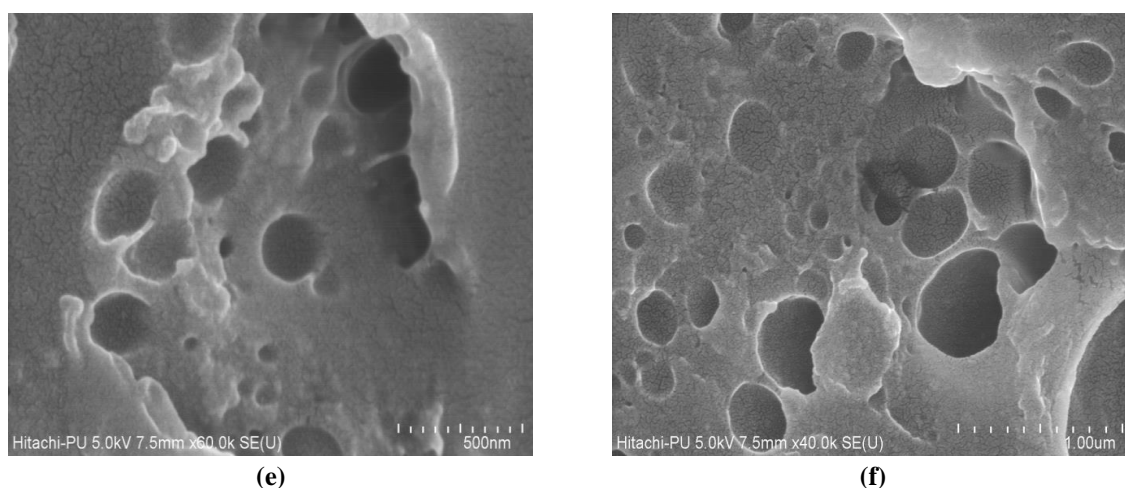
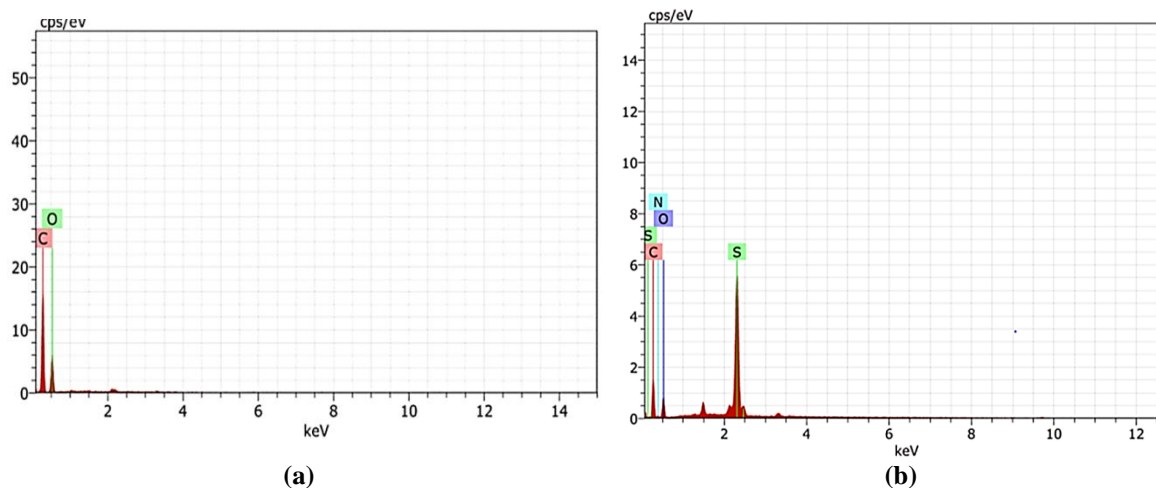


Figure 2. (a,b) FESEM images of B^{gr} ; (c,d) FESEM images of micro-poly-(Amp)-cl- B^{gr} -IV microgel; (e,f) FESEM images of DOX-loaded-micro-poly-(Amp)-cl- B^{gr} -IV.

The planar surface of B^{gr} with no prominent morphological features was revealed from FESEM studies (Figures 2a and 2b). After polymerisation and cross-linking with AMPSA, a substantial variance in the morphology of the microgel was observed. Figures 2c and 2d depict the formation of three-dimensional networks with N, N'-MBA, resulting in a highly porous structure with a pore size between 50-150 nm. However, the FESEM scans of DOX-loaded micro-poly-(Amp)-cl- B^{gr} -IV (Figures 2e and 2f) showed fewer pores as the major fraction of these pores gets occupied with DOX molecules. Thus, FESEM data confirms the significant cross-linking in micro-poly-(Amp)-cl- B^{gr} -IV and the sufficient uptake of DOX by it.

3.2.3. EDS analysis.

The EDS analysis was performed to determine the elemental make-up of B^{gr} , micro-poly-(Amp)-cl- B^{gr} -IV, and DOX-loaded-micro-poly-(Amp)-cl- B^{gr} -IV. The EDS pattern of B^{gr} shows the peaks of C (59.05 wt% and 65.76 atom%) and O (40.95 wt% and 34.24 atom%) (Figure 3a). Micro-poly-(Amp)-cl- B^{gr} -IV, displayed a reduction in wt% and atom% of O (16.60 % to 16.06 %), accompanied by the induction of an additional peak of N at 0.2 KeV and S at 2.2 KeV (Figure 3b). These additional peaks of N and S verify the successful incorporation of AMPSA into barley. The EDS done for DOX-loaded-micro-poly-(Amp)-cl- B^{gr} -IV (Figure 3c) depicts an increase in atom% and wt% of S and C from 61.70 % to 72.35 %, and 16.57 % to 7.29 %, respectively. The wt% and atom% of N also witnessed an increase (8.87 % to 8.94 %) in DOX-loaded micro-poly-(Amp)-cl- B^{gr} -IV, and such an increase further confirms the considerable uptake of DOX by the microgel.



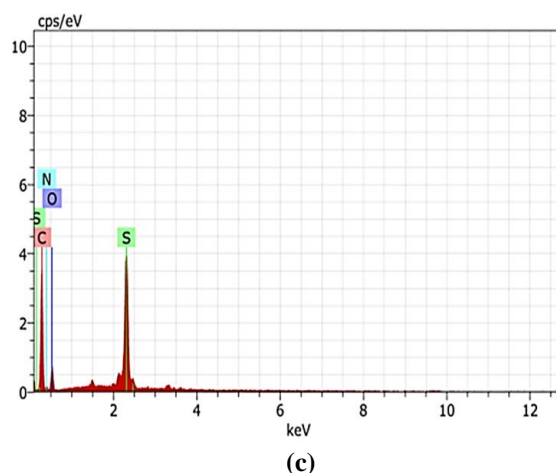


Figure 3. (a)EDS spectra of B^{gr}; (b) micro-poly-(Amp)-cl-B^{gr}-IV; (c) DOX-loaded-micro-poly-(Amp)-cl-B^{gr}-IV.

3.2.4. TEM analysis and dynamic-light scattering studies.

Furthermore, micro-poly-(Amp)-cl-B^{gr}-IV was analysed using TEM studies (Figures 4a and 4b). TEM studies revealed the rough porous surface of the microgel. The analysis confirms the micro-size distribution of microgels within the 100-500 nm range.

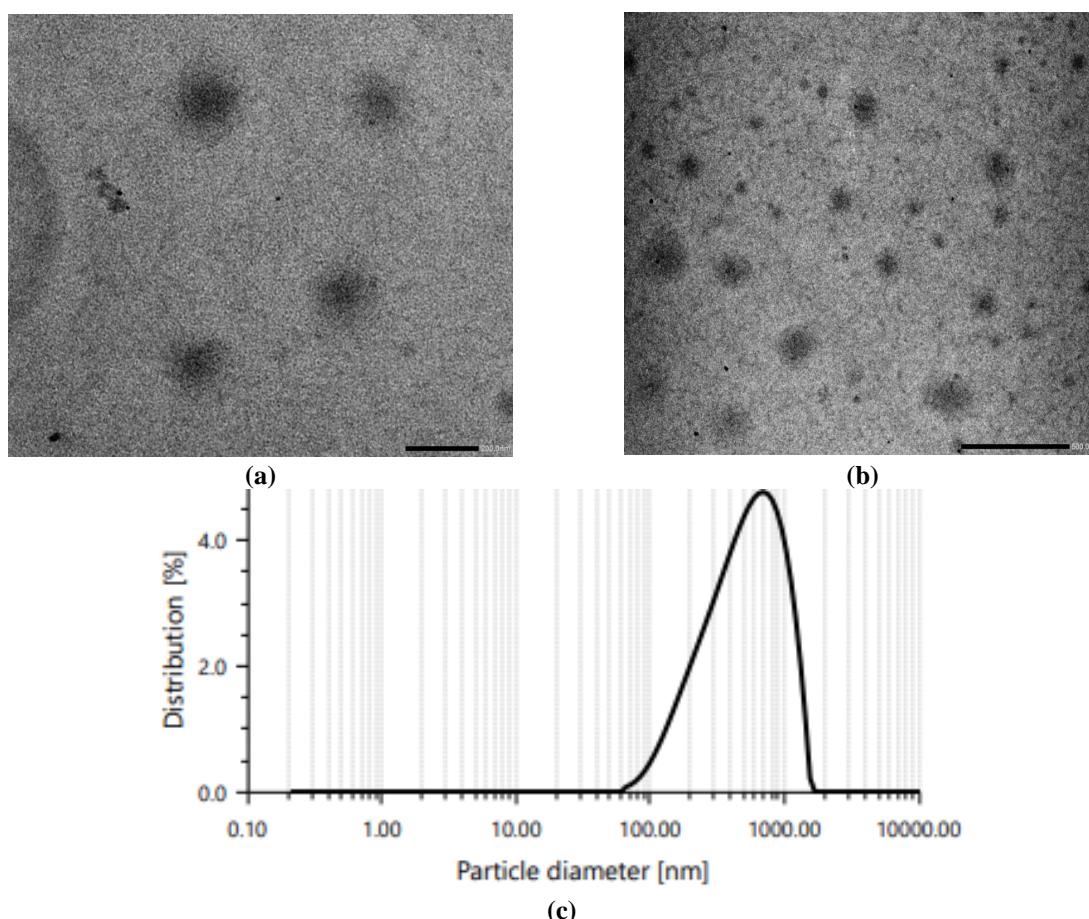


Figure 4. TEM images of (a) micro-poly-(Amp)-cl-B^{gr}-IV (200 nm); micro-poly-(Amp)-cl-B^{gr}-IV (500 nm); (c) Particle size distribution (intensity) of microgels suspended in water at 25°C.

According to DLS measurements performed at 25°C with 1mg/mL microgel dispersion, the synthesized microgels showed an average hydrodynamic diameter of 462.8 nm. This gives a fair idea of micro-sized distribution within the range of 100-500 nm of swollen microgels suspended in water. DLS further provides the particle size distribution peaks around 500 nm.

The DLS-based particle size analysis confirms the major fraction of microgels having a range of diameters suspended in the water around 500 nm within the few hundred nanometres to micrometre-sized hydrogels or cross-linked networks range (1-1000 nm) [62]. Fig.4c shows the graphical representation of the variation of hydrodynamic diameter with particle size distribution (intensity).

3.2.5. XRD analysis.

The synthesis of micro-poly-(Amp)-cl-B^{gr}-IV distorts the crystalline structure of B^{gr}, and the amorphous phase was thus observed in the XRD pattern of micro-poly-(Amp)-cl-B^{gr}-IV. In the XRD pattern of B^{gr}, the diffraction plot is differentiated by the broad 2θ peak at 20.10° which becomes a bit broader with reduced intensity in the XRD pattern of micro-poly-(Amp)-cl-B^{gr}-IV (Figure 5) which further confirms the incorporation of AMPSA onto the backbone since after cross-linking the crystalline region is disrupted. The surface becomes more amorphous [63].

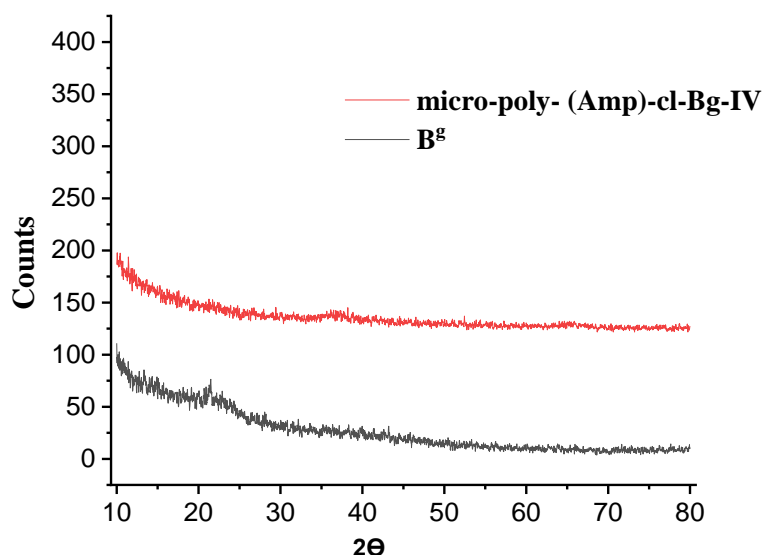


Figure 5. XRD spectra of B^{gr} and micro-poly-(Amp)-cl-B^{gr}-IV.

3.3. Swelling studies.

3.3.1. Impact of time on percent swelling (P_s).

Figure 6a depicts the effect of time on P_s. There is a continuous increase in P_s of micro-poly(Amp)-cl-B^{gr}-IV with time, and a maximum swelling of 8686% was observed within 210 min at 25°C, which becomes constant after that. This can be explained based on the occupation of pores with water molecules till 210 min and the non-availability of vacant pores after that. Thus, no further increase in swelling was observed thereafter [64].

3.3.2. Impact of temperature on P_s.

Figure 6b showcases the P_s dependence on micro-poly-(Amp)-cl-B^{gr}-IV. The dependence of swelling on temperature was predicted by observing P_s at different temperatures (20-55°C), at a preoptimized time of 210 min. The swelling increased with temperature, with a maximum swelling of 16,239% at 45°C, whereas the swelling at 37°C was found to be 14,449%. At low temperatures, the hydrogen bonding among the polymer molecules and neighbouring water molecules resulted in decreased interaction with microgels. As the

temperature rises, the weakening of the hydrogen bonding results in increased thermal mobility of the water molecules and their interaction with microgels and the increased P_s . The decrease in P_s above 45°C can be attributed to desorption due to disintegration at higher temperatures [65].

3.3.3. Impact of pH on P_s .

Figure 6c depicts the pH-responsive nature of the microgel. The swelling pattern of micro-poly-(Amp)-*cl*-B^{gr}-IV was monitored at different pH levels of aqueous media (2.2, 5.5, 6.8, 7.4, 9.2, and 10.0) at optimised time and temperature, i.e., 210 min and 45°C. pH-responsive behaviour of synthesised microgel was demonstrated through swelling studies in different pH media, and swelling order was found in the order: 5.5>6.8>7.4>2.2>9.2>10.0. At acidic pH, due to protonation of $-\text{SO}_3\text{H}$ groups, the hydrogen bonding decreased considerably and thus decreased swelling. In an alkaline medium, the interaction of the $-\text{SO}_3\text{H}$ group with water is restricted by basic moieties present in the solution and on the sample surface [66]. Whereas, in the neutral media, no such hindrances occur on the surface of microgels, and $-\text{SO}_3\text{H}$ groups get well solvated to give appreciable swelling to microgels. Such swelling behaviour of the DOX-carrying platform supports DOX delivery in the tumour environment.

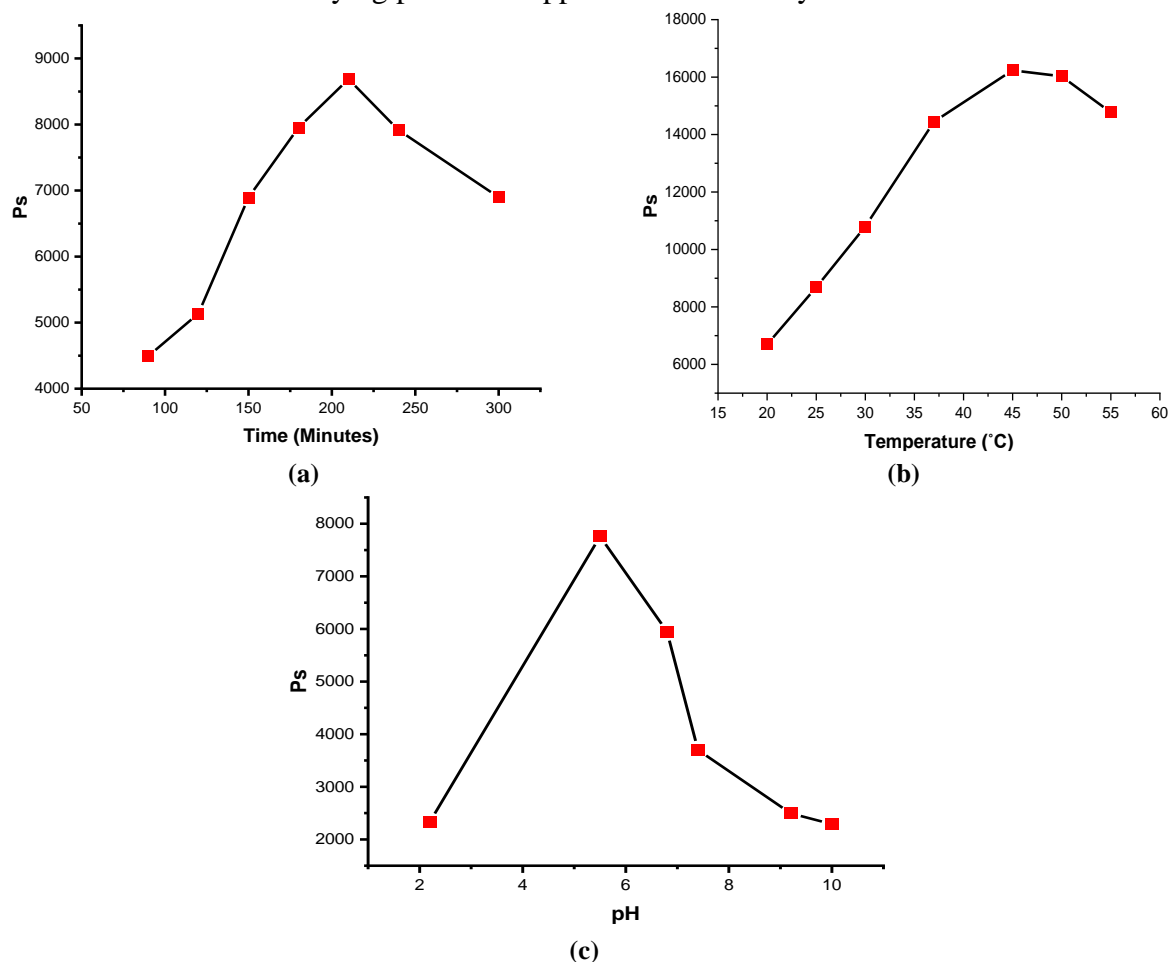


Figure 6. (a) Effect of time on P_s of micro-poly-(Amp)-*cl*-B^{gr}-IV at pH-7.0 and 25°C; (b) Effect of temperature on P_s of micro-poly-(Amp)-*cl*-B^{gr}-IV at pH-7.0 and 210 min; (c) Effect of pH on P_s of micro-poly-(Amp)-*cl*-B^{gr}-IV at 45°C and 210 min.

The swelling pattern of micro-poly-(Amp)-*cl*-B^{gr}-IV confirmed its pH-sensitive nature with substantial swelling of 7759% at pH 5.5, 5950% at pH 6.8, and 3700% at pH 7.4. Thus, the synthesised microgel can act as a suitable and ideal matrix for anticancer drug delivery.

3.4. DOX delivery studies.

DOX delivery studies include the loading and release of DOX under varied pH conditions. The $\text{-SO}_3\text{H}$ groups present on the microgel skeleton were employed for the binding of DOX with the hydrogel *via* electrostatic interactions. The $\text{-SO}_3\text{H}$ groups provide affinity to microgels towards the basic -NH_2 group of DOX. Other polar groups, such as carbonyl groups present in DOX, increase its interactions with microgels.

3.4.1. DOX loading studies.

A DOX solution of concentration 300 mg/L was prepared in double-distilled water due to the high aqueous solubility of DOX. 100 mg of sample was immersed in DOX solution, and the drug loading of the sample was determined spectrophotometrically at 495 nm after regular intervals. The maximum %uptake of 92.23% was observed in 300 min (Figure 7a). DOX uptake was confirmed by UV-spectral studies as absorbance for DOX concentration decreases with time. This appreciable loading tendency of hydrogel for DOX makes it an effective and competent drug-delivery device [67].

3.4.2. Drug (DOX) release studies.

The *in vitro* release pattern of DOX was explored at varied physiological media having pHs of 5.5, 6.8, and 7.4. The pHs are selected specifically to imitate the intracellular compartments (lysosomes and endosomes, pH 5.5), the extracellular compartment (pH 6.8) in the tumour tissues, and the biological pH of blood (pH 7.4) in normal tissue. The quantity of DOX liberated was examined using a UV-visible spectrophotometer at a λ_{max} of 498 nm against the standard curve. The discharge of DOX from the DOX-loaded matrix was affected by pH changes. The drug release was 93.5%, 57.6%, and 36.4% at pH 5.5, 6.8, and 7.4 within 72h (Figure 7b). The DOX release was found at its lowest at physiological pH 7.4, corresponding to normal cells' pH, and maximum for acidic pH 5.5 found at cancerous endosomes and lysosomes. This is a positive aspect of this study as the normal cells will be least affected by the drug, and the drug will affect only the cancer cells. Also, the drug loss during its route to the targeted site will be countered.

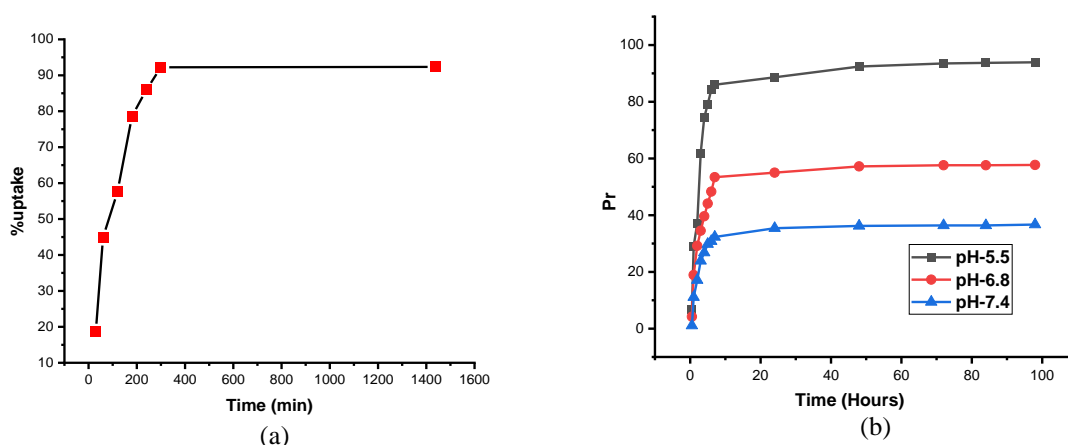


Figure 7. (a) Effect of time on the DOX uptake using micro-poly-(Amp)-cl-B^{gr}-IV at 25°C and pH 7.4; (b) Effect of time on DOX release %age (Pr) using [DOX]-loaded micro-poly-(Amp)-cl-B^{gr}-IV at 37°C.

Therefore, drug dosage can be properly managed as errors due to drug loss will be diminished, and this will further ensure the exact therapeutic dose at the targeted site. This will also reduce the effects linked to high drug concentration administered, considering the drug loss up to the targeted site.

3.4.3. DOX release kinetics.

The mechanism and kinetics of DOX release from microgels were investigated using Zero-order, First-order, Higuchi, and Korsmeyer-Peppas kinetic models (Figures 8a-d). The model with the highest correlation coefficient (R^2) value was considered the best-fit model (Table 3).

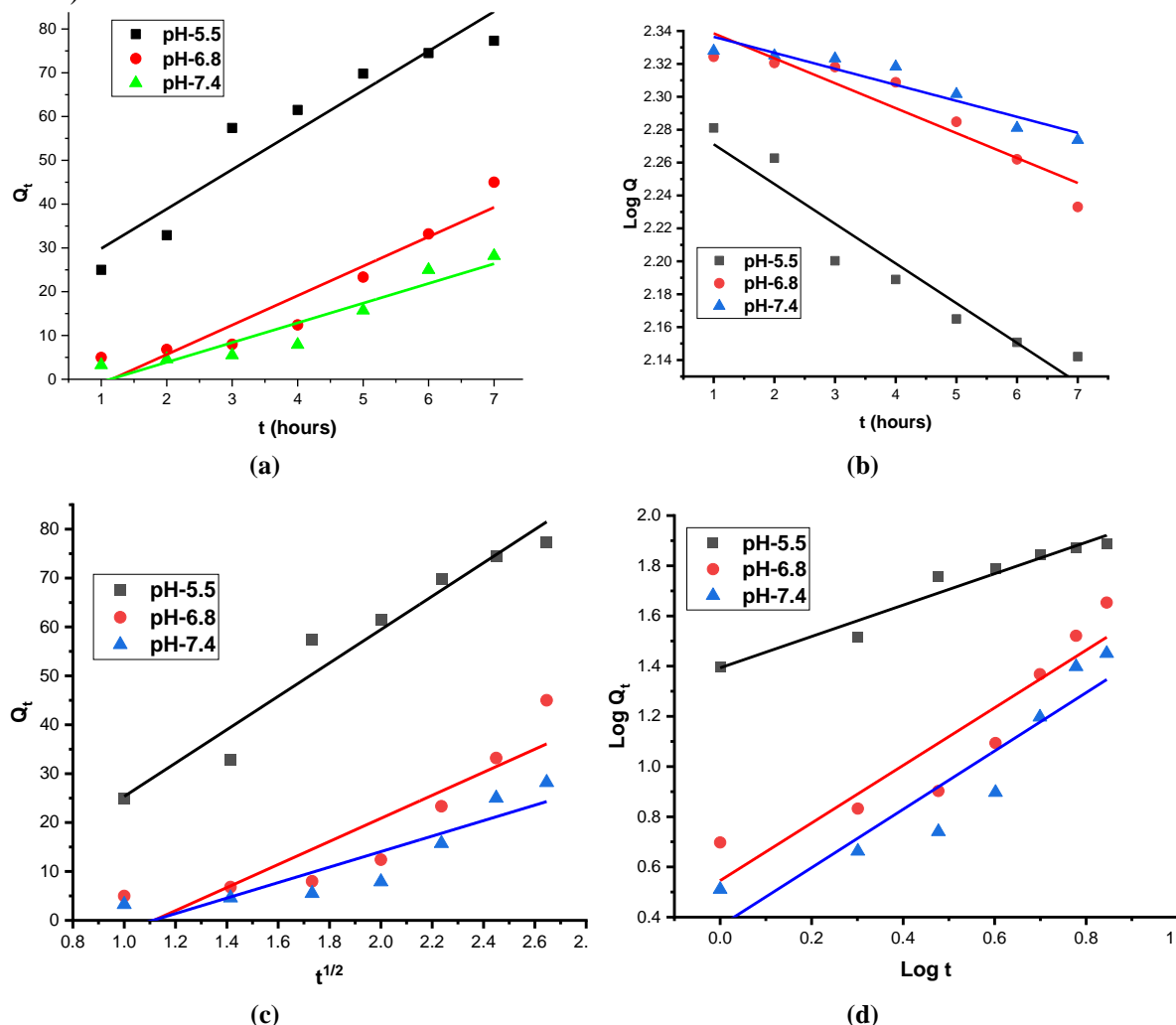


Figure 8. (a) Zero-order; (b) First-order; (c) Higuchi; (d) Korsmeyer-Peppas kinetic model for DOX release at 37°C and pH-5.5, 6.8, and 7.4.

Table 3. Parameters calculated from release kinetic models.

Kinetic models	Parameters	pH-5.5	pH-6.8	pH-7.4
Zero-Order	R^2	0.889	0.859	0.867
	K_0	9.16	6.79	4.49
First-Order	R^2	0.942	0.865	0.871
	K_1	0.01	0.006	0.02
Higuchi	R^2	0.931	0.773	0.778
	K_H	34.11	23.57	15.8
Korsmeyer-Peppas	R^2	0.941	0.837	0.838
	K_{KP}	19.95	3.46	2.39
	n	0.6	0.98	1.0

Table 3 revealed that the First-Order kinetic model is the best-suited model for DOX release with a maximum R^2 of 0.942, 0.865, and 0.871 at pH-5.5, 6.8, and 7.4, respectively. This demonstrates that the controlled dissolution of water-soluble doxorubicin from the porous surface of microgel is dependent on the concentration of the drug absorbed by it [68]. The 'n' values of 0.6, 0.98, and 1.0 at pH 5.5, 6.8, and 7.4 reflect non-Fickian diffusion involved in the release mechanism [69]. This can be attributed to the tendency of microgels to imbibe a large amount of solvent and swell up considerably in the DOX solution, followed by the eruption of the matrix.

3.4.4. *In vitro* cytotoxic studies.

The cytotoxicity of DOX-loaded micro-poly(Amp)-*cl*-B^{gr}-IV was evaluated using the A549 human lung cancer cell line. Normally, A549 cells are pebble-shaped, but on treatment with DOX-loaded micro-poly(Amp)-*cl*-B^{gr}-IV, their normal shape gets distorted, thus causing their death [70]. The cytotoxicity of micro-poly(Amp)-*cl*-B^{gr}-IV was found to be concentration-dependent (Figure 9). At the optimum concentration of DOX, the normal pebble-shaped A549 cells get distorted and become somewhat spherical. They showed maximum cell viability at pH 5.5. Thus, the synthesized microgel acts efficiently against cancerous cells in a sustained and controlled manner.

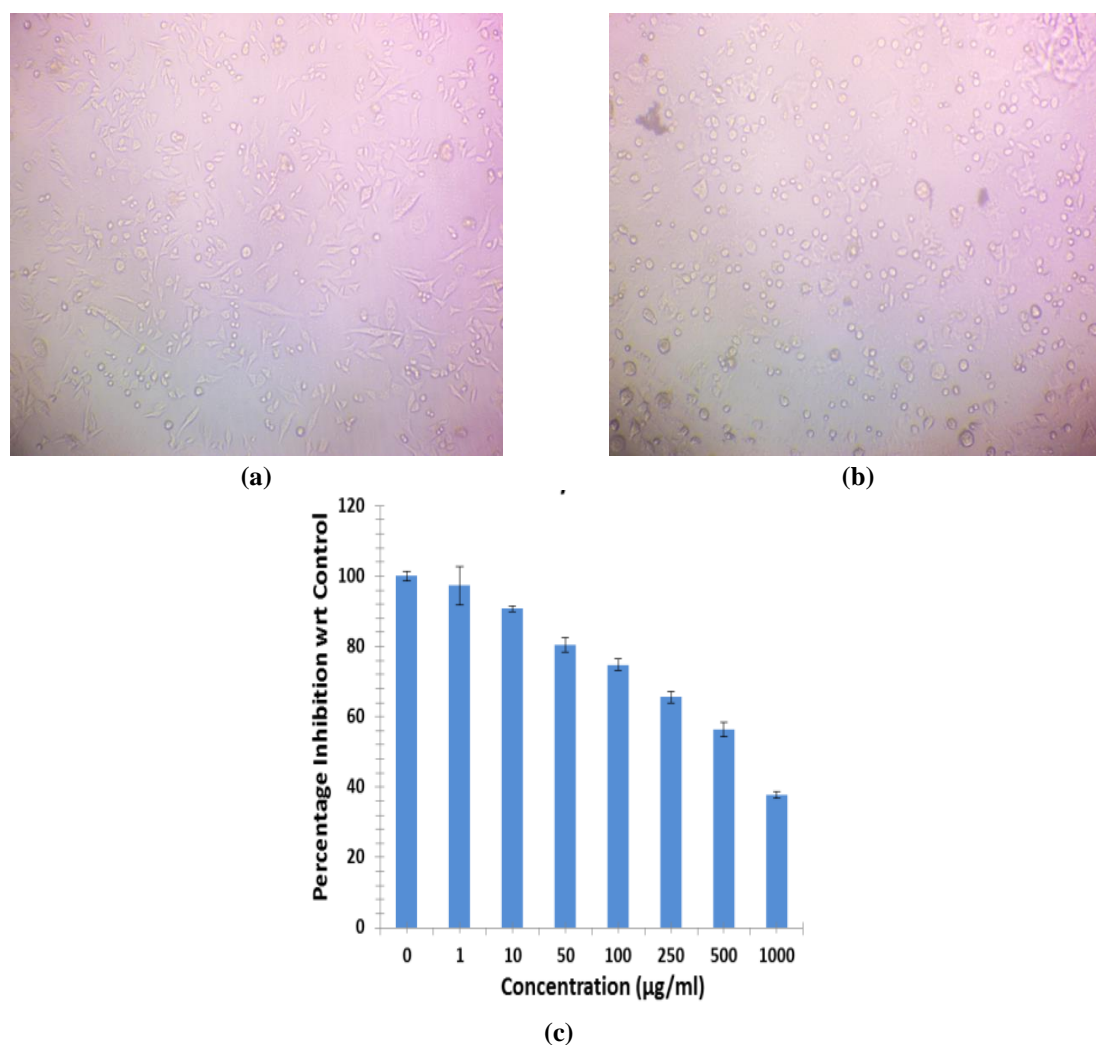


Figure 9. Images of (a) A549 cells treated at pH-5.5 with 10 µg/mL concentration; (b) A549 cells treated at pH-5.5 with 503 µg/mL; (c) in vitro cell viability of A549 cell lines treated with different concentrations.

Cytotoxicity studies were conducted to evaluate the therapeutic efficacy of Doxorubicin-loaded microgels. To assess their performance relative to free doxorubicin, the IC₅₀ values of the microgel formulation were compared with those of free doxorubicin, as reported in recent peer-reviewed publications. IC₅₀ calculated for free doxorubicin comes around 10 µg/mL [71]. The comparative analysis revealed that the Doxorubicin-loaded microgels exhibited cytotoxic effects consistent with their drug content, while the unloaded microgels themselves showed no inherent cytotoxicity, confirming their biocompatibility and suitability as a drug delivery platform. The lower IC₅₀ value observed for the drug-loaded microgels compared to the free doxorubicin indicates enhanced therapeutic efficacy. This improvement may be attributed to the ability of the microgels to provide sustained and controlled release of the drug, thereby maintaining effective intracellular concentrations over a longer duration. Additionally, the use of microgels may contribute to reduced systemic toxicity by facilitating targeted delivery and minimizing drug exposure to healthy tissues. The IC₅₀ value calculated for DOX-loaded microgels was 497 µg/mL.

4. Conclusions

The present study dealt with the *in-vacuum* synthesis of the pH-responsive microgels using whole grain barley (*Hordeum vulgare* L.) and AMPSA via the radical method, followed by sonication and centrifugation. The synthetic parameters optimized for the synthesized micro-poly-(Amp)-*cl*-B^{gr}-IV were 200 mmHg, 75°C in 50 min. The swelling studies depicted the superabsorbent behaviour of the microgel with a maximum swelling of 16,239% at 45°C. The microgel was further evaluated as a loading and delivery device for DOX. Microgel exhibited a significant loading capacity for DOX (92.23%). The release behaviour of DOX-loaded microgel was found to be pH-controlled with a maximum release of 93.5% at pH 5.5 and a least release of 36.4% at pH 7.4 within 72 h of release time. This behaviour of the matrix is highly desirable to diminish the drug loss and side effects related to high concentrations of drugs during its route to the targeted site. The cytotoxicity studies performed on the A549 human lung cancer cell line further revealed the potential anticancer activity of the loaded microgels. Thus, the synthesized pH-responsive microgels can be categorized as an ideal matrix for the site-specific controlled delivery of DOX for the treatment of cancer.

Author Contributions

Conceptualization, K.K., G.S.C., and S.C.; methodology, S.R.; investigation, A.R. and S.R.; data curation, S.R.; writing—original draft preparation, A.R.; writing—review and editing, K.K., G.S.C., and S.C.; supervision, K.K.; co-supervision, S.C.; project administration, K.K.; All authors have read and agreed to the published version of the manuscript.

Data Availability Statement

Data will be made available on request.

Funding

This research received no external funding.

Acknowledgments

The authors are thankful to the Department of Chemistry, Himachal Pradesh University, Shimla, H.P., India, for providing necessary chemicals, laboratory, and instrumentation facilities for carrying out this research work.

Conflicts of Interest

The authors declare no conflict of interest.

References

1. Rashid, A.B.; Kausik, M.D.A.K. AI revolutionizing industries worldwide: A comprehensive overview of its diverse applications. *Hybrid Adv.* **2024**, *7*, 100277, <https://doi.org/10.1016/j.hybadv.2024.100277>.
2. Deo, S.V.S.; Sharma, J.; Kumar, S. GLOBOCAN 2020 Report on Global Cancer Burden: Challenges and Opportunities for Surgical Oncologists. *Ann. Surg. Oncol.* **2022**, *29*, 6497-6500, <https://doi.org/10.1245/s10434-022-12151-6>.
3. Wong, M.C.S.; Ding, H.; Wang, J.; Chan, P.S.F.; Huang, J. Prevalence and risk factors of colorectal cancer in Asia. *Intest. Res.* **2019**, *17*, 317-329, <https://doi.org/10.5217/ir.2019.00021>.
4. Yan, C.; Shan, F.; Ying, X.; Li, Z. Global burden prediction of gastric cancer during demographic transition from 2020 to 2040. *Chin. Med. J.* **2023**, *136*, 397-406, <https://doi.org/10.1097/CM9.0000000000002626>.
5. Mathur, P.; Sathishkumar, K.; Chaturvedi, M.; Das, P.; Sudarshan, K.L.; Santhappan, S.; Nallasamy, V.; John, A.; Narasimhan, S.; Roselind, F.S.; null, n. Cancer Statistics, 2020: Report From National Cancer Registry Programme, India. *JCO Global Oncol.* **2020**, 1063-1075, <https://doi.org/10.1200/GO.20.00122>.
6. Kulsh, J. Biochemistry—Not Oncogenes—May Demystify and Defeat Cancer. *Oncol. Ther.* **2023**, *11*, 154-169, <https://doi.org/10.1007/s40487-023-00221-y>.
7. Warenus, H.M. The essential molecular requirements for the transformation of normal cells into established cancer cells, with implications for a novel anti-cancer agent. *Cancer Rep.* **2023**, *6*, e1844, <https://doi.org/10.1002/cnr2.1844>.
8. Rajput, S.; Sharma, P.K.; Malviya, R. Fluid mechanics in circulating tumour cells: Role in metastasis and treatment strategies. *Med. Drug Discov.* **2023**, *18*, 100158, <https://doi.org/10.1016/j.medidd.2023.100158>.
9. Al-Ostoot, F.H.; Salah, S.; Khanum, S.A. An Overview of Cancer Biology, Pathophysiological Development and It's Treatment Modalities: Current Challenges of Cancer anti-Angiogenic Therapy. *Cancer Invest.* **2024**, *42*, 559-604, <https://doi.org/10.1080/07357907.2024.2361295>.
10. Chinnadurai, R.K.; Khan, N.; Meghwanshi, G.K.; Ponne, S.; Althobiti, M.; Kumar, R. Current research status of anti-cancer peptides: Mechanism of action, production, and clinical applications. *Biomed. Pharmacother.* **2023**, *164*, 114996, <https://doi.org/10.1016/j.biopha.2023.114996>.
11. Wu, W.; Pu, Y.; Shi, J. Nanomedicine-enabled chemotherapy-based synergetic cancer treatments. *J. Nanobiotech.* **2022**, *20*, 4, <https://doi.org/10.1186/s12951-021-01181-z>.
12. Ganesh, K.; Massagué, J. Targeting metastatic cancer. *Nat. Med.* **2021**, *27*, 37-44, <https://doi.org/10.1038/s41591-020-01195-4>.
13. Oltulu, Ç.; Türker, N.P. Effect of L-Dopa on Carboplatin Induced Hepatotoxicity. *Int. J. Innov. Approaches Sci. Res.* **2023**, *7*, 37-46, <https://doi.org/10.29329/ijiasr.2023.524.4>.
14. Al-Ali, H.M.; Al-Asadi, J.N.; Alrubaye, A.; Ali, H.M.H. Ototoxicity in Cancer Patients on Cisplatin Therapy Attending Basrah Oncology Centre: A Cohort Study. *Iraqi. Natl. J. Med.* **2023**, *5*, 29-37, <https://doi.org/10.37319/inqjm.5.2.2>.
15. Fekete, J.T.; Györfy, B. New Transcriptomic Biomarkers of 5-Fluorouracil Resistance. *Int. J. Mol. Sci.* **2023**, *24*, 1508, <https://doi.org/10.3390/ijms24021508>.
16. Salerno, L.; Notaro, A.; Consoli, V.; Affranchi, F.; Pittalà, V.; Sorrenti, V.; Vanella, L.; Giuliano, M.; Intagliata, S. Evaluation of the anticancer effects exerted by 5-fluorouracil and heme oxygenase-1 inhibitor hybrids in HTC116 colorectal cancer cells. *J. Enzyme Inhib. Med. Chem.* **2024**, *39*, 2337191, <https://doi.org/10.1080/14756366.2024.2337191>.

17. Buchtova, T.; Lukac, D.; Skrott, Z.; Chroma, K.; Bartek, J.; Mistrik, M. Drug–Drug Interactions of Cannabidiol with Standard-of-Care Chemotherapeutics. *Int. J. Mol. Sci.* **2023**, *24*, 2885, <https://doi.org/10.3390/ijms24032885>.
18. Zhao, J.; Zhang, N.; Ma, X.; Li, M.; Feng, H. The dual role of ferroptosis in anthracycline-based chemotherapy includes reducing resistance and increasing toxicity. *Cell Death Discov.* **2023**, *9*, 184, <https://doi.org/10.1038/s41420-023-01483-1>.
19. Kciuk, M.; Gielecińska, A.; Mujwar, S.; Kołat, D.; Kałuzińska-Kołat, Ż.; Celik, I.; Kontek, R. Doxorubicin—An Agent with Multiple Mechanisms of Anticancer Activity. *Cells* **2023**, *12*, 659, <https://doi.org/10.3390/cells12040659>.
20. Podyacheva, E.; Toropova, Y. Nicotinamide Riboside for the Prevention and Treatment of Doxorubicin Cardiomyopathy. Opportunities and Prospects. *Nutrients* **2021**, *13*, 3435, <https://doi.org/10.3390/nu13103435>.
21. Jenča, A.; Mills, D.K.; Ghasemi, H.; Saberian, E.; Jenča, A.; Karimi Forood, A.M.; Petrášová, A.; Jenčová, J.; Jabbari Velisdeh, Z.; Zare-Zardini, H. Herbal therapies for cancer treatment: a review of phytotherapeutic efficacy. *Biol. Targets Ther.* **2024**, *18*, 229–255, <https://doi.org/10.2147/BTT.S484068>.
22. Okoro, C.O.; Fatoki, T.H. A Mini Review of Novel Topoisomerase II Inhibitors as Future Anticancer Agents. *Int. J. Mol. Sci.* **2023**, *24*, 2532, <https://doi.org/10.3390/ijms24032532>.
23. Cheng, Z.; Li, M.; Dey, R.; Chen, Y. Nanomaterials for cancer therapy: current progress and perspectives. *J. Hematol. Oncol.* **2021**, *14*, 85, <https://doi.org/10.1186/s13045-021-01096-0>.
24. Eslami, M.; Memarsadeghi, O.; Davarpanah, A.; Arti, A.; Nayernia, K.; Behnam, B. Overcoming Chemotherapy Resistance in Metastatic Cancer: A Comprehensive Review. *Biomedicines* **2024**, *12*, 183, <https://doi.org/10.3390/biomedicines12010183>.
25. Ruman, U.; Fakurazi, S.; Masarudin, M.J.; Hussein, M.Z. Nanocarrier-based therapeutics and theranostics drug delivery systems for next generation of liver cancer nanodrug modalities. *Int. J. Nanomed.* **2020**, *15*, 1437–1456, <https://doi.org/10.2147/IJN.S236927>.
26. Theyagarajan, K.; Sruthi, V.P.; Satija, J.; Senthilkumar, S.; Kim, Y.-J. Materials and design strategies for the electrochemical detection of antineoplastic drugs: Progress and perspectives. *Mater. Sci. Eng. R: Rep.* **2024**, *161*, 100840, <https://doi.org/10.1016/j.mser.2024.100840>.
27. Jiang, H.; Zuo, J.; Li, B.; Chen, R.; Luo, K.; Xiang, X.; Lu, S.; Huang, C.; Liu, L.; Tang, J.; Gao, F. Drug-induced oxidative stress in cancer treatments: Angel or devil? *Redox Biol.* **2023**, *63*, 102754, <https://doi.org/10.1016/j.redox.2023.102754>.
28. Asqarov, A.N.; Bekmirzaeva, N.B.; Usmanova, Z.U. MAIN SIDE EFFECTS OF ANTITUMOR CHEMOTHERAPY. *Int. Bull. Med. Sci. Clin. Res.* **2023**, *3*, 107–109, <https://doi.org/10.5281/zenodo.7785349>.
29. Keziah, D.; Bindhiya, M.; Jayaprakash, M.; Prudence, R.A. Prospective observational study on the risk factors of chemotherapy-induced myelosuppression and its management in a tertiary care hospital. *Indian J. Med. Paediatr. Oncol.* **2024**, *45*, 416–421, <https://doi.org/10.1055/s-0043-1770905>.
30. Panda, J.; Nongbet, A.; Avula, S.K.; Nayak, D.; Rustagi, S.; Panda, B.P.; Mohanta, Y.K. Macro-fungi mediated nanoparticles for sustainable agriculture: recent advancement and future strategies. *Discov. Sustain.* **2025**, *6*, 375, <https://doi.org/10.1007/s43621-025-01219-4>.
31. Ranote, S.; Musioł, M.; Kowalczyk, M.; Joshi, V.; Chauhan, G.S.; Kumar, R.; Chauhan, S.; Kumar, K. Functionalized *Moringa oleifera* Gum as pH-Responsive Nanogel for Doxorubicin Delivery: Synthesis, Kinetic Modelling and In Vitro Cytotoxicity Study. *Polymers* **2022**, *14*, 4697, <https://doi.org/10.3390/polym14214697>.
32. Zhao, X.; Liu, L.; Li, X.; Zeng, J.; Jia, X.; Liu, P. Biocompatible Graphene Oxide Nanoparticle-Based Drug Delivery Platform for Tumor Microenvironment-Responsive Triggered Release of Doxorubicin. *Langmuir* **2014**, *30*, 10419–10429, <https://doi.org/10.1021/la502952f>.
33. Moriya, G.; Mazumder, R.; Padhi, S.; Mishra, R. GASTRORENTENTIVE HYDROGELS RESPONSIVE TO EXTERNAL STIMULI FOR NOVEL DRUG DELIVERY. *Int J. Appl. Pharm.* **2024**, *16*, 1–14, <https://doi.org/10.22159/ijap.2024v16i4.51051>.
34. Zhang, X.; Liang, Y.; Huang, S.; Guo, B. Chitosan-based self-healing hydrogel dressing for wound healing. *Adv. Colloid Interface Sci.* **2024**, *332*, 103267, <https://doi.org/10.1016/j.cis.2024.103267>.
35. Alharbi, H.Y.; Alnoman, R.B.; Aljohani, M.S.; Al-Anazia, M.; Monier, M. Synthesis and characterization of gellan gum-based hydrogels for drug delivery applications. *Int. J. Biol. Macromol.* **2024**, *258*, 128828, <https://doi.org/10.1016/j.ijbiomac.2023.128828>.

36. Choi, H.; Choi, W.-S.; Jeong, J.-O. A Review of Advanced Hydrogel Applications for Tissue Engineering and Drug Delivery Systems as Biomaterials. *Gels* **2024**, *10*, 693, <https://doi.org/10.3390/gels10110693>.
37. Harsányi, A.; Kardos, A.; Xavier, P.; Campbell, R.A.; Varga, I. A Novel Approach for the Synthesis of Responsive Core–Shell Nanogels with a Poly(N-Isopropylacrylamide) Core and a Controlled Polyamine Shell. *Polymers* **2024**, *16*, 2584, <https://doi.org/10.3390/polym16182584>.
38. Mehraji, S.; Saadatmand, M.; Eskandari, M. Production of letrozole-loaded alginate oxide-gelatin microgels using microfluidic systems for drug delivery applications. *Int. J. Biol. Macromol.* **2024**, *263*, 129685, <https://doi.org/10.1016/j.ijbiomac.2024.129685>.
39. Karg, M.; Pich, A.; Hellweg, T.; Hoare, T.; Lyon, L.A.; Crassous, J.J.; Suzuki, D.; Gumerov, R.A.; Schneider, S.; Potemkin, I.I.; Richtering, W. Nanogels and Microgels: From Model Colloids to Applications, Recent Developments, and Future Trends. *Langmuir* **2019**, *35*, 6231–6255, <https://doi.org/10.1021/acs.langmuir.8b04304>.
40. Li, X.; Liu, J.; Qiu, N. Cyclodextrin-Based Polymeric Drug Delivery Systems for Cancer Therapy. *Polymers* **2023**, *15*, 1400, <https://doi.org/10.3390/polym15061400>.
41. Mackiewicz, M.; Dagdelen, S.; Waleka-Bargiel, E.; Karbarz, M. A polyampholyte core-shell microgel as an environmentally sensitive drug carrier. *Arab. J. Chem.* **2024**, *17*, 105464, <https://doi.org/10.1016/j.arabjc.2023.105464>.
42. Farag, M.A.; Xiao, J.; Abdallah, H.M. Nutritional value of barley cereal and better opportunities for its processing as a value-added food: a comprehensive review. *Crit. Rev. Food Sci. Nutr.* **2022**, *62*, 1092–1104, <https://doi.org/10.1080/10408398.2020.1835817>.
43. Abebaw, G. Review on Structure, Functional and Nutritional Composition of Barley (*Hordeum vulgare*). *J. Nutr. Food Process.* **2021**, *4*, 1–8, <https://doi.org/10.31579/2637-8914/046>.
44. Qaiser, R.; Pervaiz, F.; Shoukat, H.; Yasin, H.; Hanan, H.; Murtaza, G. Mucoadhesive chitosan/polyvinylpyrrolidone-co-poly (2-acrylamide-2-methylpropane sulphonic acid) based hydrogels of captopril with adjustable properties as sustained release carrier: Formulation design and toxicological evaluation. *J. Drug Deliv. Sci. Technol.* **2023**, *81*, 104291, <https://doi.org/10.1016/j.jddst.2023.104291>.
45. Tassw, D.F.; Tesfaye, T.; Babu K, M. Preparation and Characterization of Protein-Based Hydrogel: Cottonseed Protein Grafted with 2-Acrylamido-2-Methylpropanesulfonic Acid (AMPS). *Adv. Mater. Sci. Eng.* **2024**, *2024*, 6783165, <https://doi.org/10.1155/2024/6783165>.
46. Srivastava, H.; Waigaonkar, S.; Chauhan, R. Surface modification of human hair by grafting poly(methyl methacrylate). *Polym. Bull.* **2022**, *79*, 11013–11050, <https://doi.org/10.1007/s00289-021-03990-6>.
47. Hiremath, J.N.; Vishalakshi, B. Evaluation of a pH-responsive guar gum-based hydrogel as adsorbent for cationic dyes: kinetic and modelling study. *Polym. Bull.* **2015**, *72*, 3063–3081, <https://doi.org/10.1007/s00289-015-1453-x>.
48. Heidari, S.; Mohammadi, M.; Esmailzadeh, F.; Mowla, D. Determination of Swelling Behavior and Mechanical and Thermal Resistance of Acrylamide–Acrylic Acid Copolymers under High Pressures and Temperatures. *ACS Omega* **2021**, *6*, 23862–23872, <https://doi.org/10.1021/acsomega.1c02638>.
49. Khodir, W.K.W.A.; Ismail, M.W.; Hamid, S.A.; Daik, R.; Susanti, D.; Taher, M.; Guarino, V. Synthesis and Characterization of Ciprofloxacin Loaded Star-Shaped Polycaprolactone–Polyethylene Glycol Hydrogels for Oral Delivery. *Micromachines* **2023**, *14*, 1382, <https://doi.org/10.3390/mi14071382>.
50. Mochalova, E.N.; Egorova, E.A.; Komarova, K.S.; Shipunova, V.O.; Khabibullina, N.F.; Nikitin, P.I.; Nikitin, M.P. Comparative Study of Nanoparticle Blood Circulation after Forced Clearance of Own Erythrocytes (Mononuclear Phagocyte System-Cytoblockade) or Administration of Cytotoxic Doxorubicin- or Clodronate-Loaded Liposomes. *Int. J. Mol. Sci.* **2023**, *24*, 10623, <https://doi.org/10.3390/ijms241310623>.
51. Bin Mobarak, M.; Islam, M.N.; Chowdhury, F.; Uddin, M.N.; Hossain, M.S.; Mahmud, M.; Akhtar, U.S.; Tanvir, N.I.; Rahman, A.F.M.M.; Ahmed, S. Calcined chicken eggshell-derived biomimetic nano-hydroxyapatite as a local drug-delivery aid for doxycycline hyclate: characterization, bio-activity, cytotoxicity, antibacterial activity and in vitro release study. *RSC Adv.* **2023**, *13*, 36209–36222, <https://doi.org/10.1039/D3RA07010G>.
52. Jayachandran, P.; Ilango, S.; Suseela, V.; Nirmaladevi, R.; Shaik, M.R.; Khan, M.; Khan, M.; Shaik, B. Green Synthesized Silver Nanoparticle-Loaded Liposome-Based Nanoarchitectonics for Cancer Management: In Vitro Drug Release Analysis. *Biomedicines* **2023**, *11*, 217, <https://doi.org/10.3390/biomedicines11010217>.

53. Yanar, S.; Kasap, M.; Kanli, A.; Akpinar, G.; Sarihan, M. Proteomics analysis of meclofenamic acid-treated small cell lung carcinoma cells revealed changes in cellular energy metabolism for cancer cell survival. *J. Biochem. Mol. Toxicol.* **2023**, *37*, e23289, <https://doi.org/10.1002/jbt.23289>.
54. Liu, Y.; Mao, J.; Huang, Y.; Qian, Q.; Luo, Y.; Xue, H.; Yang, S. Pt-Chitosan-TiO₂ for Efficient Photocatalytic Hydrogen Evolution via Ligand-to-Metal Charge Transfer Mechanism under Visible Light. *Molecules* **2022**, *27*, 4673, <https://doi.org/10.3390/molecules27154673>.
55. Hamad, M.T.M.H.; Saied, M.S.S. Kinetic studies of Congo red dye adsorption by immobilized *Aspergillus niger* on alginate. *Appl. Water Sci.* **2021**, *11*, 35, <https://doi.org/10.1007/s13201-021-01362-z>.
56. Raudhatussyarifah, R.; Sediawan, W.B.; Azis, M.M.; Hartati, I. Microcrystalline cellulose production by acid hydrolysis of hydrotropic rice straw pulp. *IOP Conf. Ser.: Earth Environ. Sci.* **2022**, *963*, 012055, <https://doi.org/10.1088/1755-1315/963/1/012055>.
57. Uddin, I. Onsite visual detection of heavy metal contaminants using impregnated strip. *J. Photochem. Photobiol. A Chem.* **2021**, *421*, 113512, <https://doi.org/10.1016/j.jphotochem.2021.113512>.
58. Li, M.; Karboune S.; Light, K.; Kermasha, S. Oxidative cross-linking of potato proteins by fungal laccases: Reaction kinetics and effects on the structural and functional properties. *Innov. Food Sci. Emerg. Technol.* **2021**, *71*, 102723, <https://doi.org/10.1016/j.ifset.2021.102723>.
59. El-Sayed, N.S.; Moussa, M.A.; Kamel, S.; Turky, G. Development of electrical conducting nanocomposite based on carboxymethyl cellulose hydrogel/silver nanoparticles@polypyrrole. *Synth. Met.* **2019**, *250*, 104–114, <https://doi.org/10.1016/j.synthmet.2019.03.010>.
60. Suhail, M.; Xie, A.; Liu, J.-Y.; Hsieh, W.-C.; Lin, Y.-W.; Minhas, M.U.; Wu, P.-C. Synthesis and In Vitro Evaluation of Aspartic Acid Based Microgels for Sustained Drug Delivery. *Gels* **2022**, *8*, 12, <https://doi.org/10.3390/gels8010012>.
61. Anirudhan, T.S.; Manasa, A.M. Novel pH/reduction responsive graphene oxide nanoparticles based hydrogel for targeted combination chemotherapy. *Int. J. Polym Mater. Polym. Biomater.* **2021**, *70*, 231–245, <https://doi.org/10.1080/00914037.2019.1706513>.
62. Chaudhary, J.; Thakur, S.; Sharma, M.; Gupta, V.K.; Thakur, V.K. Development of Biodegradable Agar-Agar/Gelatin-Based Superabsorbent Hydrogel as an Efficient Moisture-Retaining Agent. *Biomolecules* **2020**, *10*, 939, <https://doi.org/10.3390/biom10060939>.
63. León, O.; Soto, D.; Antúnez, A.; Fernández, R.; González, J.; Piña, C.; Muñoz-Bonilla, A.; Fernandez-García, M. Hydrogels based on oxidized starches from different botanical sources for release of fertilizers. *Int. J. Biol. Macromol.* **2019**, *136*, 813–822, <https://doi.org/10.1016/j.ijbiomac.2019.06.131>.
64. Elkony, A.; Ibrahim, A.G.; Abu El-Farah, M.H.; Abd-Elhai, F. Synthesis and characterization of (AAm-co-AHPS)/MMT hydrogel composites for the efficient capture of methylene blue from aqueous solution. *Al-Azhar Bull. Sci.* **2020**, *2020*, 31–46, <https://doi.org/10.21608/absb.2020.39315.1079>.
65. Akalin, G.O.; Pulat, M. Preparation and Characterization of Nanoporous Sodium Carboxymethyl Cellulose Hydrogel Beads. *J. Nanomater.* **2018**, *2018*, 9676949, <https://doi.org/10.1155/2018/9676949>.
66. Wang, Y.; Shi, X.; Wang, W.; Wang, A. Synthesis, characterization, and swelling behaviors of a pH-responsive CMC-g-poly(AA-co-AMPS) superabsorbent hydrogel. *Turk. J. Chem.* **2013**, *37*, 149–159.
67. Biglione, C.; Neumann-Tran, T.M.P.; Kanwal, S.; Klinger, D. Amphiphilic micro- and nanogels: Combining properties from internal hydrogel networks, solid particles, and micellar aggregates. *J. Polym. Sci.* **2021**, *59*, 2665–2703, <https://doi.org/10.1002/pol.20210508>.
68. Kariminia, S.; Shamsipur, M.; Barati, A. Fluorescent folic acid-chitosan/carbon dot for pH-responsive drug delivery and bioimaging. *Int. J. Biol. Macromol.* **2024**, *254*, 127728, <https://doi.org/10.1016/j.ijbiomac.2023.127728>.
69. Ahnfelt, E.; Sjögren, E.; Hansson, P.; Lennernäs, H. In Vitro Release Mechanisms of Doxorubicin From a Clinical Bead Drug-Delivery System. *J. Pharm. Sci.* **2016**, *105*, 3387–3398, <https://doi.org/10.1016/j.xphs.2016.08.011>.
70. Sharma, A.; Shambhwani, D.; Pandey, S.; Singh, J.; Lalhlenmawia, H.; Kumarasamy, M.; Singh, S.K.; Chellappan, D.K.; Gupta, G.; Prasher, P.; Dua, K.; Kumar, D. Advances in Lung Cancer Treatment Using Nanomedicines. *ACS Omega* **2023**, *8*, 10–41, <https://doi.org/10.1021/acsomega.2c04078>.
71. Gupta, S.; Choudhary, D.K.; Sundaram, S. Green Synthesis and Characterization of Silver Nanoparticles Using *Citrus sinensis* (Orange peel) Extract and Their Antidiabetic, Antioxidant, Antimicrobial and Anticancer Activity. *Waste Biomass Valor.* **2025**, *16*, 1101–1114, <https://doi.org/10.1007/s12649-024-02782-z>.

Publisher's Note & Disclaimer

The statements, opinions, and data presented in this publication are solely those of the individual author(s) and contributor(s) and do not necessarily reflect the views of the publisher and/or the editor(s). The publisher and/or the editor(s) disclaim any responsibility for the accuracy, completeness, or reliability of the content. Neither the publisher nor the editor(s) assume any legal liability for any errors, omissions, or consequences arising from the use of the information presented in this publication. Furthermore, the publisher and/or the editor(s) disclaim any liability for any injury, damage, or loss to persons or property that may result from the use of any ideas, methods, instructions, or products mentioned in the content. Readers are encouraged to independently verify any information before relying on it, and the publisher assumes no responsibility for any consequences arising from the use of materials contained in this publication.